1 Introduction

1.1 The ALICE experiment

ALICE (A Large Ion Collider Experiment) [1] is an experiment at the Large Hadron Collider (LHC) optimized for the study of heavy-ion collisions, at a centre of mass energy ~ 5.5 TeV. The prime aim of the experiment is to study in detail the behaviour of matter at high densities and temperatures, in view of probing deconfinement and chiral symmetry restoration.

The detector consists essentially of two main components: the central part, composed of detectors mainly devoted to the study of hadronic signals and dielectrons in the pseudorapidity range $-1 < \eta < 1$, and the forward muon spectrometer, devoted to the study of quarkonia behaviour in dense matter. The layout of the ALICE set-up is shown in colour Fig. 1.i. The first technical challenge is imposed by the large number of particles created in the collisions of lead ions. There is a considerable spread in the presently available predictions for the multiplicity of charged particles produced in a central Pb–Pb collision. The design of the experiment has been based on the highest value, 8000 charged particles per unit of rapidity, at mid rapidity. This multiplicity dictates the granularity of the detectors and their optimal distance from the colliding beams.

The detailed characterization of ion–ion collisions requires particles to be measured and identified over a large range of momenta and masses. This second challenge has determined the rather complex particle identification scheme of ALICE, as described in the next section.

1.2 Particle identification in ALICE and the HMPID

The goals of ALICE involving particle identification are: the measurement of global event characteristics like event topology, momentum spectra of identified particles, particle correlations (HBT), and particle ratios; the measurement of the ϕ decay in the KK channel; the detection of charm. The ALICE PID system has three detectors that participate in the particle identification with a full coverage of the central ALICE barrel — ITS, TPC and TOF — and a single-arm detector, the High-Momentum Particle IDentification (HMPID), devoted to the identification of the high-momentum particles, i.e. pions, kaons and protons in the range from 1 to 5 GeV/c.

The ITS and TPC identify, via the dE/dx measurement, up to $p \sim 600$ MeV/c while the TOF will cover up to 1.2–1.4 GeV/c, overlapping well with the dE/dx detectors. These detectors will allow the measurement of several signals on an event-by-event basis.

The HMPID is devoted to the detection of the particles in the momentum range above the one covered by the other detectors. Since for most particles the expected yield is rather low above $p \sim 1$ GeV/c, the HMPID is conceived as a single-arm detector that measures the spectra of particles in an inclusive manner, with the possibility to build classes of events using the event-by-event characterization done at lower momenta by the barrel detectors. The axonometric view of the HMPID detector in the ALICE set-up, together with the spaceframe that supports the HMPID, the TPC, and the time-of-flight barrel, is shown in colour Fig. 1.ii.

Not many detectors can provide the required momentum range for particle identification in the ALICE central barrel. We can envisage to use either a time-of-flight with very good time resolution (≤ 100 ps) or a ring-imaging technique using Cherenkov light. Since the time-of-flight alternative, using scintillators and photomultipliers, is both onerous and difficult in the radiation and magnetic environment of ALICE and since no other method is for the time being capable of similar resolutions, we have decided to adopt a

RICH, for which a specific R&D project has been developed (see Chapter 2). The specificity of this detector is that it employs for the first time, in a detector of that size, the concept of two-dimensional electronic readout with CsI photocathodes for the conversion of the Cherenkov photons. The high readout rate of this detector also allows particle identification at much higher rates than foreseen for Pb–Pb collisions, an important feature for the pp operation.

In Fig. 1.1 we show the front and lateral views of the HMPID, including some relevant geometrical dimensions.

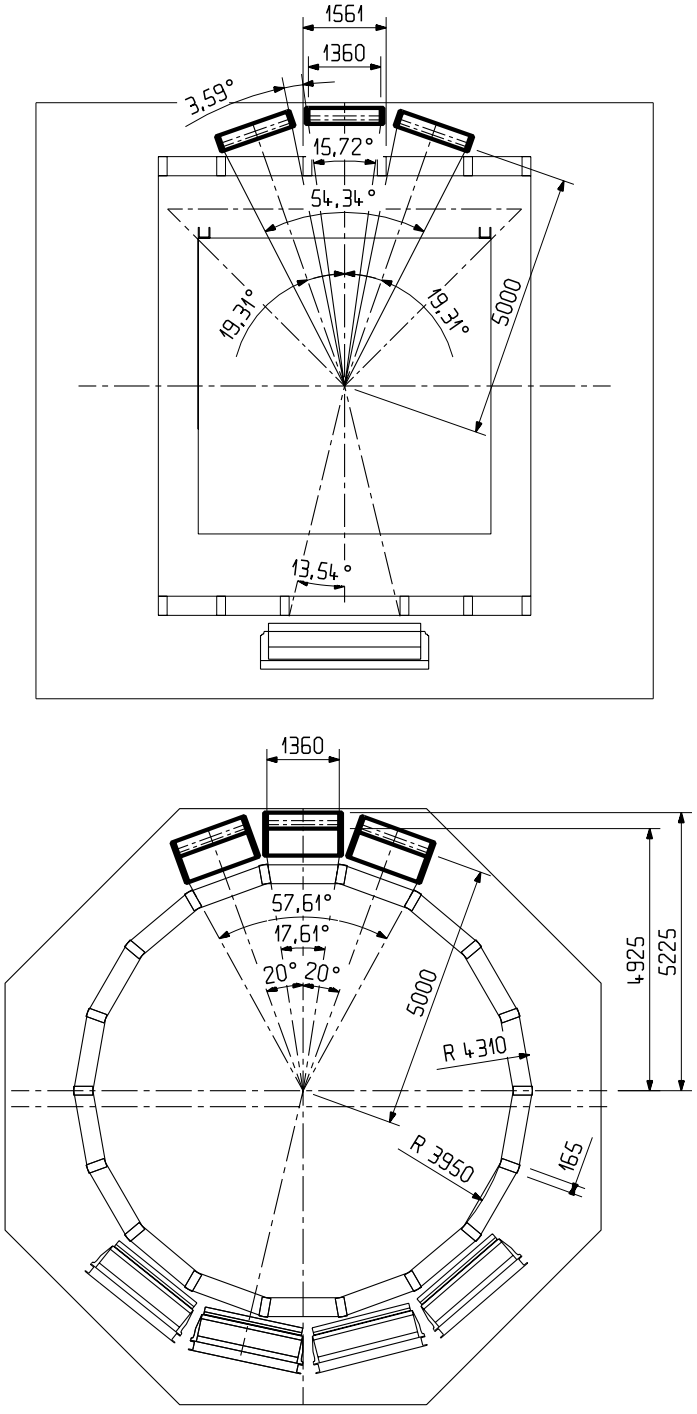

Figure 1.1: Side and front view of the HMPID, shown in the upper part of the figures. The boxes in the lower parts represent the PHOS calorimeter.

1.3 Physics of the HMPID

While the low-p_{t} particle spectra (up to around 1 GeV/c) provide information about the temperature of the formed medium, through thermal particle emission, in the high-p_{t} region, accessible through the HMPID, particle production becomes dominated by hard processes. This is a particularly interesting observable since initial hard production can be calculated in the framework of perturbative QCD, and the calculations can be verified using the data collected in pp collisions.

Detailed information on the density of the medium produced in a Pb–Pb collision can, in principle, be obtained by studying the energy loss of high-energy partons traversing that medium. Partons are usually studied, in pp collisions, via jets using calorimetry. In heavy-ion collisions, the background from the underlying event makes jet recognition difficult and leads to a bad energy resolution for jets with less than $\sim$ 100 GeV. Furthermore, the lost energy is mainly carried by soft gluons radiated close to the jet axis, making calorimetry measurements rather insensitive to jet quenching.

There is, however, an alternative way to study this interesting phenomenon. The suppression of large E_{t} jets naturally leads to the suppression of large p_{t} particles. A clear advantage of this method is the large production rate of such particles. Therefore, the measurement of the momentum spectra of identified particles at large momenta allows, with a moderate experimental effort, the study of the effect of jet quenching. The comparison of the high-p_{t} spectra of identified particles measured in Pb–Pb collisions with the calculated curves, and with the spectra obtained from pp data, will be very sensitive to the medium-induced energy loss of high-energy partons [2].

Figure 1.2a illustrates the drastic effect of jet quenching on the the proton p_{t} distribution, made visible through the ratio between the Pb–Pb and the pp spectra.

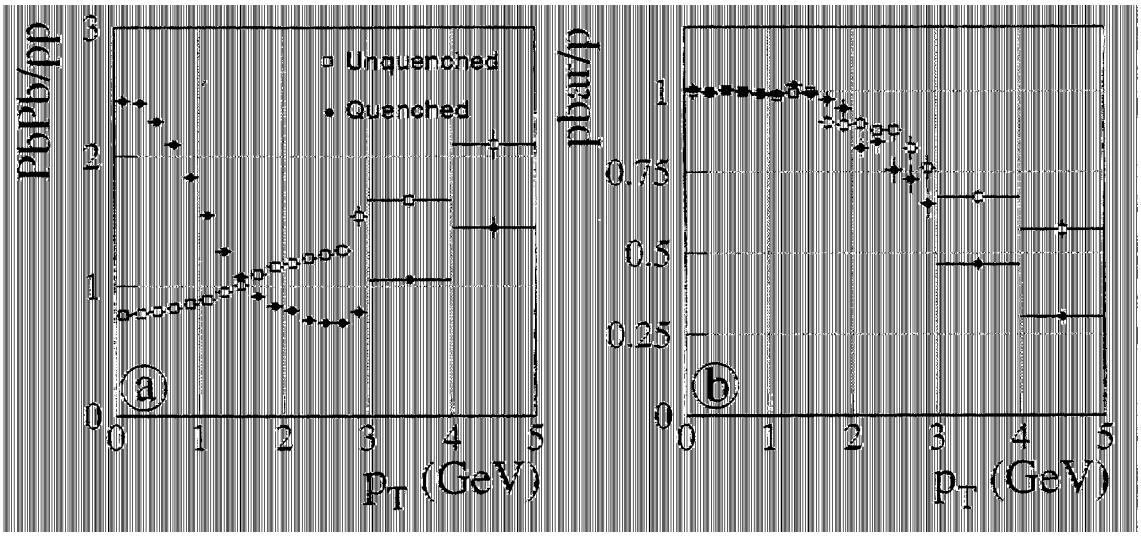

Figure 1.2: Expected influence of jet quenching on the ratio of proton p_{t} spectra between Pb–Pb and pp collisions (a) and on $\overline{\mathrm{p}}/\mathrm{p}$ ratio in Pb–Pb collisions (b). The statistics corresponds to 10^7 pp and 5×10^4 central Pb–Pb collisions.

The comparison of proton and antiproton spectra will also give information on the jet quenching in dense matter [3] . At high p_{t} the origin of the proton and antiproton spectra are not the same. The quark jets (containing more likely a valence quark) lead more often to proton than antiproton production, while the gluon jets have equal probability to produce either particle. Therefore, the protons and antiprotons may be used to 'tag' the quark and gluon jets, respectively. To that basic asymmetry in production is added the fact that the gluons, owing to their larger colour charge, lose more energy in a dense medium than quarks, thus suppressing the antiproton spectra at large p_{t}. The predicted difference in yields above 3 GeV/c is about a factor of two (see Fig. 1.2b), easily accessible by the HMPID performance.

The study of particle correlations at high momenta gives information on the evolution of the size of the emitting source as a function of the transverse mass of the different particles. This is of particular importance since the correlations in expanding systems provide information about the dynamical evolution of the system, e.g. proper time of decoupling, duration of particle emission, and presence of collective flows. Furthermore, it is also desirable to cover the possibility for a drastic change in the measured radii at high momenta — indicating a non-equilibrated early stage with a small radius.

1.4 A Ring-Imaging Cherenkov (RICH) detector using CsI photocathode

1.4.1 General remarks

The first choice to be made when designing a RICH detector for particle identification is the type of radiator and geometry to be used. The momentum limit for particle identification determines the choice of the radiator medium.

For the momentum range of interest in ALICE (1 to 5 GeV/c), and the particles we want to identify (π, K and p), only liquids have an adequate refractive index. The type of liquid is also restricted by the range of the Cherenkov photon detection, in our case limited to the far ultraviolet photons ($\lambda \leq 200$ nm). Only one liquid, C_6F_{14}, satisfies the requirement of transparency to Cherenkov photons in this range.

As far as the geometry is concerned, there is a choice between two main types of RICH detectors:

- those with focusing properties, where the photons emitted along the track in the radiator medium are subsequently focused, usually by a mirror, onto the photon detection plane, which is at the same time the focal plane of the detector;
- those that do not use focusing devices but, instead, have a particle path through the detector which is small with respect to the distance from the radiator to the photon detection plane as shown in colour Fig. 1.iii.

In our case we are forced for several reasons — particle density, space considerations, photon absorption, etc., to choose the latter solution, called also the ‘proximity focusing’.

Another vital choice is the choice of the photon detector. Considering the surface, the price, and the particle densities involved, the only realistic candidate is a solid photocathode consisting of CsI in conjunction with a MWPC. This technique allows for a detector of considerable simplicity and adequate performance in the ALICE environment.

Although in ALICE we are confronted with high charged particle densities hitting the detector (more than 80 particles/m^2 in the highest multiplicity events), the low counting rate ($\leq 10^4$ Hz) allows a long integration time to be used on the induced charge signal. Therefore, we can operate at a rather low gas gain, particularly well suited for the CsI operation. In colour Fig. 1.iv we show an event recorded with the fully equipped prototype (proto-2) module, that represents two-thirds of the final one.

1.4.2 The HMPID layout in ALICE

The HMPID detector consists of seven modules in a calot-like arrangement at the top of the ALICE set-up as shown in Fig. 1.1. The adopted layout is dictated by physics requirements and by technical constraints. The latter will be explained in detail in Chapter 3 and we shall review here only the aspects connected to the physics. The range of positive identification (i.e. the range where the particles will emit Cherenkov light) starts at different momenta for different particle masses. For instance, the lower limit for kaon identification will be ~ 1.2 GeV/c and the lower limit for proton identification will be ~ 2 GeV/c. Both limits allow a good overlap with the capability of the time-of-flight system.

Mainly for reasons of particle density, it was important to locate the detector as far as possible from the interaction point, close to the inner radius of the L3 magnet. In order to ensure the best tracking accuracy

(see Chapter 4), no detector or constructive element is planned in between the outer wall of the TPC and the HMPID.

The size of the detector is determined by the following factors:

- the cross section for high-momentum particle production is too small to allow an event-by-event analysis: only inclusive measurements are possible;
- the measurement of correlations between high-momenta particles imposes a minimum detector size both in the beam direction and in the azimuthal angle coverage, to allow the detection of small source sizes, corresponding to rather large momentum differences in the relative momenta of the particles.

1.5 Overview of the HMPID design and main results

1.5.1 R&D, prototypes, and test results

The use of large-area CsI photocathodes as a photo-converter element in a RICH detector, as proposed for the HMPID in 1993, was a novel concept. The preliminary research work was launched in the framework of the CERN RD-26 project and a 1 m^2 prototype (proto-2) has been completed and tested in the framework of the ALICE collaboration. In the following we give an overview of the main results obtained during this period.

1.5.1.1 CsI photocathode

CsI photocathodes of large areas, up to half a square metre, can be produced with high and reliable Quantum Efficiency (QE) performance by using standard and affordable technologies:

- the substrate, that acts also as the pad-segmented cathode of a wire chamber, can be manufactured using industrial Printed Circuit Board (PCB) techniques applying specific features such as surface polishing and use of nickel layer;
- the CsI evaporation is performed using Joule effect under a vacuum of a few 10^{-6} Torr. A key improvement in QE on such substrates was obtained by post treatment, the effect of which is illustrated in Fig. 2.8 on page 21. It consists of performing the CsI evaporation on a substrate held at 60 °C, maintaining this temperature under vacuum during eight hours after evaporation.

The CsI photocathode is operated at atmospheric pressure as the cathode of a wire chamber. It was shown that the ratio between the QE value measured at atmospheric pressure and the one in vacuum is a function of the gas species and of the reduced field value at the cathode surface, E/p (V/cm Torr^{-1}). CH_4 was found to achieve the best ratio, close to 0.9, at the field value to be used in the wire chamber (see Fig. 2.6 on page 20).

1.5.1.2 Single-electron detection using CsI pad cathode in a MWPC

The chamber performs the detection of Cherenkov single photoelectrons and minimum-ionizing particles (MIP). Since a 2-dimensional readout pattern is mandatory, signals induced on pads are measured. The cathode-to-anode gap has been chosen to be 2 mm, a compromise between anode/cathode coupling, MIP primary deposition, and layout arguments. The main concern was to demonstrate a stable operation of the chamber at a gain insuring maximum photoelectron yield and maximum single-electron detection efficiency while mastering the problem of the feedback photons in a chamber with an ‘open geometry’ configuration. The number of feedback photons $N_{\rm pf}$ emitted by primary avalanches is proportional to the size of the avalanche, according to $N_{\rm pf} = k \times G$ where k is a constant depending on the gas medium and G the chamber gain. The fraction of $N_{\rm pf}$ converted by the CsI photocathode leads in cases of large

avalanches to the smearing of the Cherenkov signal and the creation of an uncorrelated background. Both effects increase the pad occupancy per ring pattern. Also, at high G diverging processes may occur when $N_{\rm pf}$ approaches 1, in case of highly ionizing events, possibly damaging the chamber. The pre-requisite to satisfy the previous requirements is to build a charge sensitive front-end electronics (see Chapter 3). Then, the choice of the operating gas is a key feature. Following gas mixtures studies, the present choice is still pure CH_4. The main results are presented, as a function of the single-electron mean pulse height in Fig. 2.36a. The lower curve shows that the mean number of Cherenkov photoelectrons reaches a plateau at a value of 16 per ring while the total number of electrons and of pad hits per event increases with the gain, as expected from feedback photon contribution. In Fig. 2.36b, one sees that the relative photon feedback yield shows a minimum at a gain in the plateau. Figure 2.35 on page 48 indicates a single-electron detection efficiency larger than 90% for A_0 above 30 ADC channels, providing a significant plateau length with stable operation. The effect of a small admixture of iC_4H_{10} in CH_4, as shown in Fig. 2.60 on page 65, results in a reduction by 50% of the feedback photon yield at high gain but a drop of 10–20% of the photoelectron yield.

We have also established that a magnetic field, up to about 1 T, parallel to the photocathode, does not affect the photoelectron yield (see Fig. 2.43 on page 54).

1.5.1.3 Results obtained with the 1 m^2 prototype (proto-2)

A full-scale prototype, representing two-thirds of a final HMPID module, was assembled and equipped with four CsI photocathodes 64×38.4 cm^2, two radiator trays, 133×41.3 cm^2, and 15 360 channels of pad front-end (FE) electronics. It was exposed at PS/SPS test beams under single- and multiparticle irradiation up to a track density locally higher than the one expected in ALICE. A large amount of data was recorded under various operating conditions for further pattern recognition studies. The operation of the chamber was very stable up to the maximum gain at which we want the detector to be operated, in an irradiation flux two orders of magnitude larger than the one expected in ALICE. The mean value of the photoelectron yield measured at the plateau for the four proto-2 photocathodes was 14.9 ± 1.5, using a 10 mm thick C_6F_{14} radiator. The uniformity of the photoelectron yield was always found satisfactory (see Fig. 2.54 on page 60).

1.5.1.4 Angular resolution of the reconstructed Cherenkov photons

The intrinsic angular resolution obtained with single-particle events was studied as a function of many parameters: chamber gain, gas species, radiator thickness, incidence angle and ring radius. Only the ring radius affects the single-photon angular resolution, as seen in Fig. 2.63 on page 69. From a radius of 100 mm, this resolution flattens at a value of 7–8 mrad. Surprisingly, all the other parameters are of little influence on this value, as seen in Figs. 2.64 on page 70, 2.65 and 2.66 on page 71. The corresponding ring resolution is of 2 mrad with a 10 mm thick radiator and particles at β close to 1.

1.5.1.5 Stability of the CsI photocathodes

During the R&D period, 32 large photocathodes (PCs) were produced and evaluated using RICH prototypes. As seen in Fig. 2.55 on page 60, a significant step in the QE performance was achieved from the 19th PC onwards, when the new pad substrate technology was adopted. The spread in QE values decreased substantially for the last produced PCs. That might reflect the greater care taken in the protection of the PCs against exposure to air during transfer and mounting on the detector. The stability of the QE as a function of time was checked on several PCs kept under continuous argon flow and evaluated at the beam periodically. A QE drop of about 5% has been observed over a four-year period (see Fig. 2.56 on page 62).

1.5.2 Detector description

In the first part of Chapter 3, the design and the prototyping studies of all the elements of a CsI-RICH module are described. The main elements of a CsI-RICH module are sketched in Fig. 1.3.

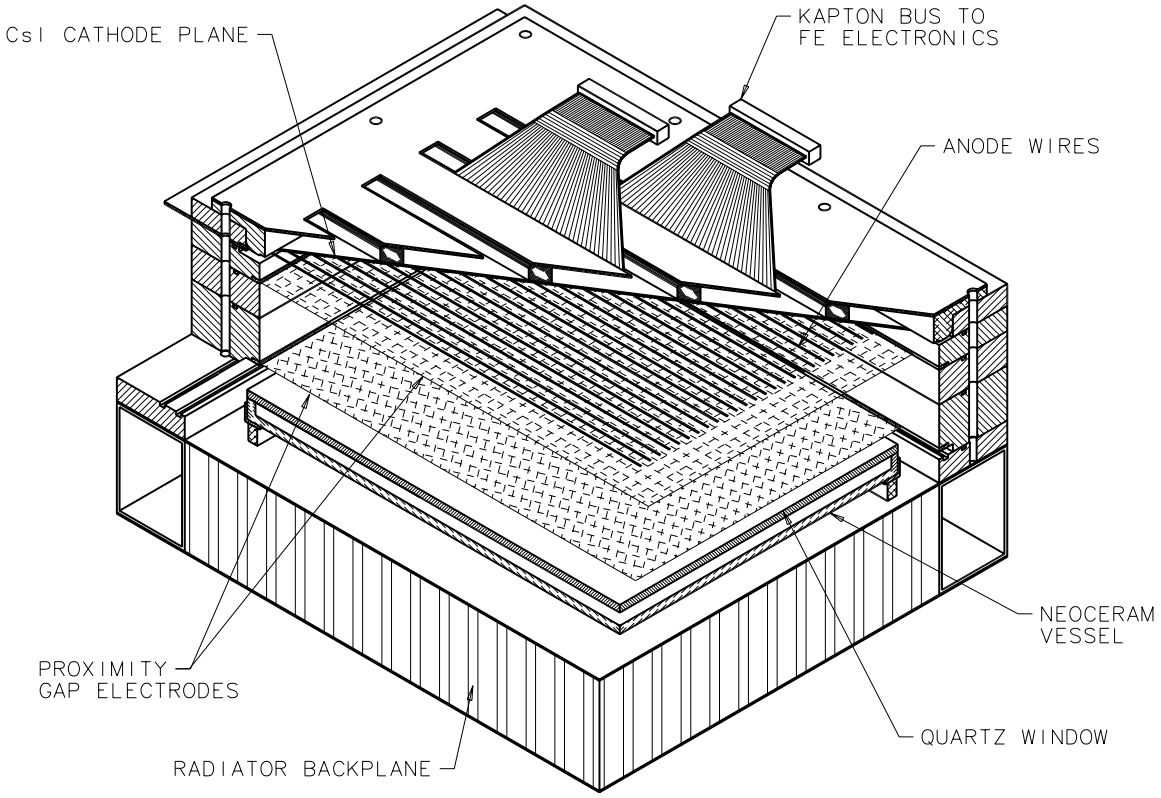

Figure 1.3: Artist's rendering of a HMPID module showing the various detector components, including the Kapton bus lines which carry the signals to the GASSIPLEX amplifiers (not shown).

- The photodetector is a conventional 2 mm gap MWPC with anode wires 20 μm in diameter and a pitch of 4 mm. One of the cathodes is a wired electrode (2 mm pitch, 100 μm diameter), while the second, where the CsI is deposited, is pad segmented. The pad size is 8×8 mm^2. The module has been designed in such a way that the CsI pad panels are stand-alone elements, easily detachable for CsI processing operations, while ensuring a reproducible and accurate chamber geometry, such as the cathode-to-anode gap of 2 mm within ± 50 μm (see Figs. 3.1 and 3.2 on page 84).
  The pad panels, made of light and stiff composite materials, hold on one face the pad PCB with the CsI layer and on the other the front-end electronics (FEE). The connections between the pads and the FEE inputs are made by flexible Kapton foils soldered at the back of the pad plane (see Figs. 3.4 and 3.5 on page 87).
- The CsI photoelectric threshold of 210 nm imposes severe UV-transmission specifications on the liquid radiator, C_6F_{14}, and on its container. The latter consists of a tray made of a glass-ceramic material with a 133×41.3 cm^2 silica window. The constituting materials have comparable dilation coefficients to ensure a perfect sealing of the glued assembly. The tray, designed to hold a hydrostatic pressure equivalent to 120 mbar, has been successfully tested up to 130 mbar.
- A C_6F_{14} circulation system has been built to purify, circulate, fill, and empty the two prototype radiator trays, remotely and safely. It is based on a gravity flow principle ensuring simple, passive, and safe operation, fully protected against overpressure.

- The front-end pad electronics has been designed by benefiting from the low interaction rate, 1–100 kHz, specific to the ALICE operation. It allows the use of a charge-sensitive preamplifier with a long integrating time, providing high sensitivity, and a multiplexed analog operation, saving digitizing channels. The system is based on the ASIC CMOS front-end chip GASSIPLEX, providing 16 analog multiplexed channels. The noise figure of the charge amplifier is 630 e r.m.s. at 0 pF. A filter stage, adapted to the long-tailed input current shape delivered by a wire chamber, ensures a base line restoration in 3 μs at 0.5% of the peak amplitude. A shaper stage sets the peaking time to 700 ns. The chip is operated in Track and Hold mode storing the charges into capacitors by means of an external trigger signal sent at the peak amplitude.
- A system has been built to evaporate the CsI by Joule effect on panels of 70×50 cm^2 and to perform the post-treatment by heating at 60 °C, under a vacuum of a few 10^{-6} Torr. The system allows the CsI photocathodes to be taken out without contact with air.
  The QE across the surface of the photocathodes can be evaluated in situ by means of a device, located in a vessel appended to the evaporation chamber, that measures the direct photocurrent emitted by local irradiation with monochromatic UV beam.

In the second part of Chapter 3, the system aspect of the HMPID is described, detailing the assembly and test procedures of the seven modules as well as the final schematics of the electronics and of the gas and liquid supplies.

1.5.3 Detector performance

We have studied the HMPID performance in the ALICE environment, under the highest particle densities currently predicted.

A complete simulation of the radiation environment of ALICE has been undertaken using the GEANT and FLUKA simulation programs, as well as the response of the RICH detectors assuming the design established in this document. The simulation shows that we shall be confronted with an important flux of charged particles, only about 30% of which is due to primary particles. The remaining part of the flux is due to secondary particles of different origins (see Table 4.2 on page 157). The neutron flux in the detector, although large, creates relatively few interactions. However, they result in an important energy deposition. Taking into account the response of the detector to charged particles and to the Cherenkov photons created in the radiator liquid and in its quartz window, the occupancy has been calculated to be about (10 ± 2)%.

We have developed a pattern recognition technique, based on a modified Hough transform method, which has been applied to samples of 'synthetic' data, created from the superposition of single events taken at the SPS, with 350 GeV/c pions at perpendicular incidence. Randomly overlapping between 10 and 50 particles/m^2, the corresponding occupancy varied from 2% to 12%. The highest value corresponds to the occupancy anticipated for the highest multiplicity ALICE events, according to the simulation.

The applied pattern recognition method was robust enough to identify the Cherenkov ring patterns and to determine the mean photon angle with satisfactory resolution. The best resolution was achieved for the smaller rings — an important indication for the final chamber design. The quality of the pattern recognition can be appreciated in Fig.1.4, for the largest occupancy expected in ALICE. The Gaussian fit gives a resolution of 6.2 mrad. Translated into identification range for π/K, it corresponds to an upper limit of 2.5 GeV/c. In the case of lower occupancies, either for more peripheral Pb–Pb collisions or for lighter nuclei (e.g. Ca–Ca), the identification limit is beyond 3 GeV/c.

We have also studied the matching of tracks recorded in the ITS and in the TPC (and extrapolated to the HMPID) with charged-particle impacts in the MWPC cathode. A matching efficiency of about 96% in the environment of 100 particles/m^2 has been achieved in the simulation.

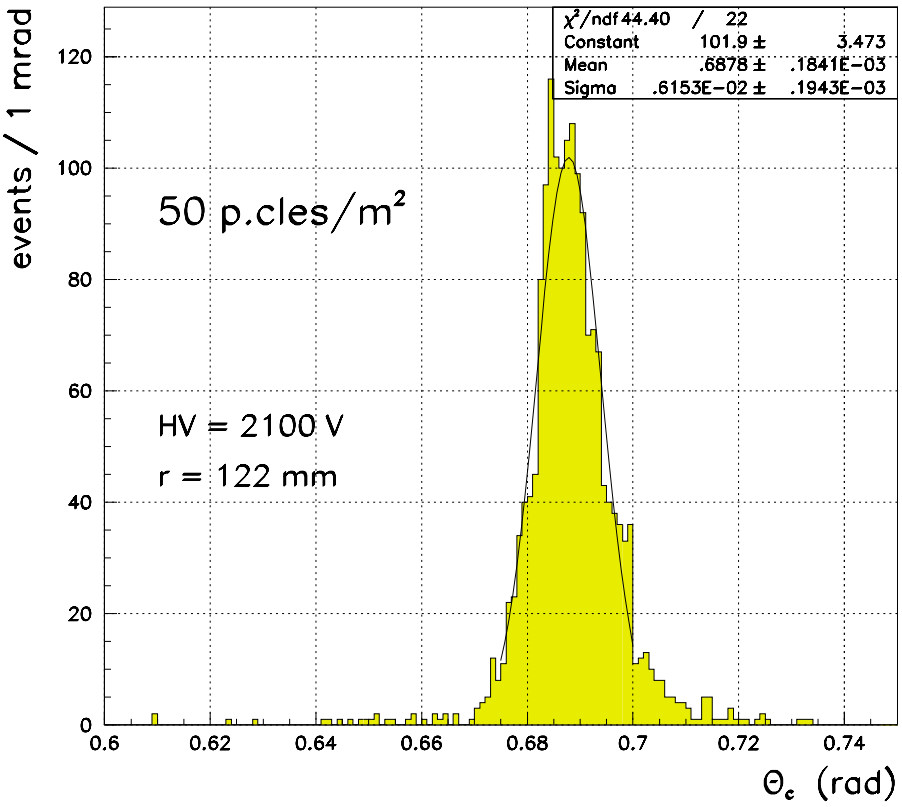

Figure 1.4: Cherenkov angle distribution at 50 particles/m^2, for the sample (4) described in Table 4.5 on page 160.

The current detector design and the performance demonstrated with a large prototype met essentially all the requirements set in the Technical Proposal [1] for the HMPID. Nevertheless, we intend to use the time available before the start of construction (in 2000) to further optimize and improve the HMPID system.

figure 1.i

figure 1.ii

figure 1.iii

figure 1.iv